Geobiology (2005), **3**, 247–260

The coupling of biological iron cycling and mineral weathering during saprolite formation, Luquillo Mountains, Puerto Rico

H. L. BUSS,[1]* M. A. BRUNS,[2] M. J. SCHULTZ,[3] J. MOORE,[1] C. F. MATHUR[3] AND S. L. BRANTLEY[1]

[1]*Department of Geosciences, The Pennsylvania State University, University Park, Pennsylvania, USA*
[2]*Department of Crop and Soil Sciences, The Pennsylvania State University, University Park, Pennsylvania, USA*
[3]*Department of Biological Sciences, York College of Pennsylvania, York, Pennsylvania, USA*

ABSTRACT

Corestones of quartz diorite bedrock in the Rio Icacos watershed in Puerto Rico weather spheroidally to form concentric sets of partially weathered rock layers (referred to here as *rindlets*) that slowly transform to saprolite. The rindlet zone (0.2–2 m thick) is overlain by saprolite (2–8 m) topped by soil (0.5–1 m). With the objective of understanding interactions between weathering, substrate availability, and resident micro-organisms, we made geochemical and microbiological measurements as a function of depth in 5 m of regolith (soil + saprolite). We employed direct microscopic counting of total cell densities; enumeration of culturable aerobic heterotrophs; extraction of microbial DNA for yield calculations; and biochemical tests for iron-oxidizing bacteria. Total cell densities, which ranged from 2.5×10^6 to 1.6×10^{10} g^{-1} regolith, were higher than 10^8 g^{-1} at three depths: in the upper 1 m, at 2.1 m, and between 3.7 and 4.9 m, just above the rindlet zone. High proportions of inactive or unculturable cells were indicated throughout the profile by very low percentages of culturable heterotrophs (0.0004% to 0.02% of total cell densities). The observed increases in total and culturable cells and DNA yields at lower depths were not correlated with organic carbon or total iron but were correlated with moisture and HCl-extractable iron. Biochemical tests for aerobic iron-oxidizers were also positive at 0.15–0.6 m, at 2.1–2.4 m, and at 4.9 m depths. To interpret microbial populations within the context of weathering reactions, we developed a model for estimating growth rates of lithoautotrophs and heterotrophs based on measured substrate fluxes. The calculations and observations are consistent with a model wherein electron donor flux driving bacterial growth at the saprolite–bedrock interface is dominated by Fe(II) and where autotrophic iron-oxidizing bacteria support the heterotrophic population and contribute to bedrock disaggregation and saprolite formation.

Received 14 October 2005; accepted 28 December 2005

Corresponding author: H. L. Buss. Tel.: 1-814-863-8055; fax: 1-814-863-8094; e-mail: buss@geosc.psu.edu

INTRODUCTION

The Rio Icacos watershed in the Luquillo Mountains of eastern Puerto Rico has one of the highest documented chemical weathering rates of granitic rocks in the world (White *et al.*, 1998). Quartz diorite of Tertiary age (Rio Blanco stock) underlies the watershed, which receives an average annual precipitation of 420 cm. Detailed physical, hydraulic, and chemical characterization of the regolith (i.e. material between the surface and the bedrock) has been conducted in the Rio Icacos watershed at sites on the Guaba Ridge (Murphy *et al.*, 1998; White *et al.*, 1998; Schulz & White, 1999). The Rio Icacos regolith consists of 50–100 cm of soil (inceptisol) above a layer of oxidized saprolite that varies in depth between 2 and 8 m (Fig. 1). Soil and saprolite are typically thinner on hill slopes and thicker on hilltops. Weathering studies of the saprolite indicate that some minerals that are abundant in the bedrock (hornblende, augite, and plagioclase) are absent in the saprolite (Murphy *et al.*, 1998; White *et al.*, 1998). Quartz and biotite are present in the bedrock as well as in the saprolite, where biotite weathers directly to kaolinite (Murphy *et al.*, 1998; Schulz & White, 1999). Although mineral weathering has been studied intensively in this regolith, the extent to which biological processes contribute to the observed rapid weathering rates has not been evaluated.

Biological processes are known to play significant roles in soil formation and surficial weathering (e.g. Richter & Markewitz, 1995). However, the contributions of biological activity to regolith and rock weathering below the root zone are less

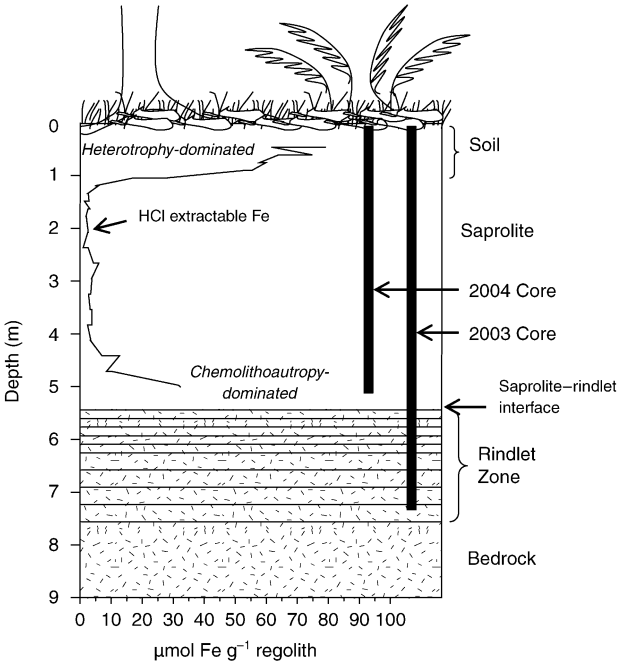

Fig. 1 Cartoon depicting the system studied in the Rio Icacos watershed. The quartz diorite bedrock is overlain with 2–8 m of saprolite and topped by 50–100 cm of soil. The bedrock weathers spheroidally, forming a zone of partially weathered rock layers termed *rindlets*. In 2003, a core was augered to 7.5 m, partially into the rindlet zone. In 2004, a core was augered to 5 m through soil and saprolite only.

well understood, especially in humid tropic forests that have shallow root systems and rapid nutrient cycling in surficial layers (e.g. Poszwa *et al.*, 2002). In the specific case of the Rio Icacos regolith, the upper soil layer is highly weathered, grading from an organic-rich A horizon (<10 cm) to a clay-enriched B horizon (~40–90 cm). Here, biological processes are indicated by evidence of roots and bioturbation by earthworms, other burrowing fauna, and root throws (White *et al.*, 1998). Below the B soil horizon, the saprolite exhibits no or very few visible signs of bioturbation.

Interestingly, fewer microbiological studies have been conducted of terrestrial near-surface environments, i.e. unsaturated zones between rooting depth and bedrock (Madsen, 1995; Fierer *et al.*, 2003) than of the deep subsurface (Amy & Haldeman, 1997; Leu *et al.*, 1998; Fredrickson & Fletcher, 2001; Lehman *et al.*, 2001). Recent investigations of granitic saprolite in Australia (Taunton *et al.*, 2000) and South Carolina (Richter & Neung-Hwan, 2002) indicate that saprolite environments can harbour a diversity of organisms (Richter & Oh, 1995). Thus, depending on cell densities, activity levels, and genetic capabilities, micro-organisms may play critical roles in geochemical transformations at depths below the rooting zone.

Some evidence for the importance of biological processes at depth is provided by mineralogical data from the saprolite–bedrock transition zone, here called the *rindlet zone* (Fig. 1). Within this zone, plagioclase and hornblende weather completely and quartz and biotite weather partially; the latter minerals continue to weather within the saprolite (Murphy *et al.*, 1998; White *et al.*, 1998). The rindlet zone is comprised of ~0.2–2 m of concentric layers of partially weathered rock called *rindlets* that surround boulders of unweathered bedrock called *corestones* (Turner *et al.*, 2003; Buss *et al.*, 2004; Fletcher *et al.*, in press). For simplicity, we will refer to the boundary between the deepest saprolite and the outermost rindlet surface as the *saprolite–bedrock interface*. Rindlets eventually disaggregate to form saprolite. Ge/Si ratios in two streams near the Guaba ridge site have shown that weathering of primary minerals in the rindlet zone controls the elemental flux out of the watershed during base flow, with weathering of the saprolite becoming dominant only during storm events (Kurtz & Derry, 2004).

If microbial densities in the Rio Icacos regolith vary with depth in relation to physical and chemical properties (e.g. mineralogy, pore water chemistry, organic carbon content, gas chemistry, hydrology), we would expect these variations to indicate corresponding changes in the bioavailability of carbon and electron donors and acceptors. Because Fe(II) is released upon weathering of hornblende and biotite, the flux of Fe(II) from the bedrock into the saprolite during weathering would supply micro-organisms with an energy alternative to organic carbon. Low carbon contents and Fe(II) availability would favour autotrophic iron-oxidizing bacteria (Hallbeck & Pedersen, 1991; Holt *et al.*, 1994). The objectives of the current study were to survey microbial distribution with depth in the Rio Icacos regolith and to propose a model for estimating relative contributions of heterotrophic and iron-oxidizing autotrophic bacteria to biological weathering of the regolith. To these ends, we obtained estimates of total, culturable, and iron-oxidizing micro-organisms, particle size distributions, moisture, and chemical concentrations in regolith samples.

METHODS

Field site and sample collection

Two regolith cores (soil + saprolite) were collected to the point of refusal by hand augering from the top of the Guaba Ridge in the Rio Icacos watershed in the Luquillo Experimental Forest. The regolith age is 200 Ka (Brown *et al.*, 1995) and is located in a lower montane wet Colorado forest with rugged topography. Soils at the collection site are grouped in the Picacho–Ciales complex (USDA NCRS, 2002), which are very deep, somewhat poorly drained soils found on the ridgetops and slopes of the Luquillo Mountains. Although the soils in this complex have been previously classified as ultisols (Boccheciamp *et al.*, 1977), they are now considered inceptisols (i.e. Picacho soils are fine-loamy,

kaolinitic, isothermic Aquic Dystrudepts) (USDA NCRS, 2002). Pore water pH of the soil and saprolite is 4.0–5.4 (White *et al.*, 1998). The augered site was approximately 1 m south of the edge of the LG-1 lysimeter field (latitude 18°16′ 54.2″N, longitude 65°47′ 25.3″W) described and mapped by others (Murphy *et al.*, 1998; White *et al.*, 1998; Turner *et al.*, 2003) and the two cores (5.7 cm diameter) were augered approximately 1 m apart, east-west (Fig. 1). Core depths were 7.5 m in June 2003 and 5.0 m in June 2004. The 2003 core was longer than the 2004 core, because the 2003 core was augered 2.5 m deeper into the rindlet zone whereas the 2004 core was not augered into this zone. Samples were removed from the auger at 0.15–0.3 m depth intervals for a total of 34 and 22 sampled depths in 2003 and 2004, respectively. Precautions were taken to avoid contamination by cleaning and wiping auger and spatula surfaces with ethanol prior to sampling and by confining analysis to samples from the inner portions of saprolite in the auger bucket. Samples were placed in sterile plastic bags. Samples were refrigerated in Puerto Rico and transported packed in blue ice within 3 days to Pennsylvania State University, where they were stored at 4 °C until analysis. Microbiological laboratory work was initiated 7 days after sample collection and was completed within an 8-week period.

Chemical and physical analyses

Bulk elemental analysis of both major and minor elements was performed by inductively coupled plasma atomic emission spectrometry (ICP-AES) after lithium metaborate fusion digestion (SGS Laboratories, Toronto, Ontario, Canada) of pulverized and sieved (150 μm) material from each of the sampled depths from 0.15 to 5 m of the 2004 core and 0.15–7.3 m of the 2003 core. Mass transfer (loss or gain from the parent rock during weathering) of individual elements relative to Zr was calculated for each sample depth (Brimhall & Dietrich, 1987). Because saprolite is isovolumetrically weathered rock, volumetric strain (change in volume as a result of stress), calculated on the basis of an assumed immobile element, should be near zero. Previously, Ti was identified as immobile in the saprolite at this site (White *et al.*, 1998); however, Zr was shown to be better conserved than Ti in the present samples. The immobility of Zr in these samples was confirmed by our calculations of very low volumetric strain with respect to Zr relative to the parent rock composition. Mass transfer (gain or loss) of an element *j*, relative to the parent rock is represented by the mass transfer coefficient, $\tau_{Zr,j}$, which is calculated as:

$$\tau_{Zr,j} = \left(\frac{\rho_w C_{j,w}}{\rho_p C_{j,p}}\right)(\varepsilon_{Zr,w} + 1) - 1, \qquad (1)$$

where ρ_w is the dry bulk density of the weathered material (saprolite and soil, White *et al.*, 1998), ρ_p is dry bulk density of the parent (*p*) rock, $C_{j,w}$ is the mass concentration of element *j* in the weathered material, $C_{j,p}$ is the mass concentration of element *j* in the parent rock, and $\varepsilon_{Zr,w}$ is the volumetric strain in the weathered (*w*) sample with respect to Zr in the parent rock:

$$\varepsilon_{Zr,w} = \frac{\rho_p C_{Zr,p}}{\rho_w C_{Zr,w}} - 1 \qquad (2)$$

If $\tau_{Zr,j} = -1$, element *j* is entirely lost. If $\tau_{Zr,j} > 0$, a net gain of element *j* relative to the parent rock is indicated. We used an average parent rock composition based on all available published compositions of the Rio Blanco quartz diorite as reported by Turner *et al.* (2003). Mass transfer in an open-system can be quantified in this manner when the parent material is homogenous (Rio Blanco quartz diorite), of uniform age (Tertiary), and contains an inert component (Zr) present in both the parent and the product material (Chadwick *et al.*, 1990).

Not all elements in a soil or saprolite matrix are expected to be easily accessible to micro-organisms. Specifically, metals such as iron that are bound in a silicate mineral lattice are significantly more refractory than iron bound in carbonate or (oxyhydr)oxide minerals, weakly adsorbed to mineral surfaces, or complexed to organic matter. These labile sources of iron would be more bioavailable than silicate-bound iron (Emerson, 2002). In soil and saprolite samples, measurement of labile iron can be accomplished by solubilization using a dilute HCl leach (modified from Sutherland, 2002; Castillo-Gonzalez & Bruns, 2005), which does not mobilize silicate lattice-bound iron. To extract the labile iron, 0.5 g of saprolite from each sampled depth (in duplicate) was carefully weighed and placed in 15 mL centrifuge tubes with 10 mL 0.5 N HCl and agitated on an end-over-end shaker at room temperature for 17 h. Samples were centrifuged at 4000 × *g* for 10 min and the supernatants were decanted into new tubes and centrifuged again before filtering (0.4 μm).

Ferrous iron in the extracts was measured in triplicate by ultraviolet-visible (UV/Vis) spectrophotometry using a standard ferrozine assay (Stookey, 1970; Gibbs, 1976). Briefly, 40 μL of the extracts were added to 2.5 mL ferrozine solution (2 mM ferrozine, 50 mM HEPES buffer) in clean cuvettes, sealed with Parafilm and vortexed to mix. Samples were allowed to react for 25 min, then absorbance at 562 nm was measured on a Spectronic 20D + UV/Vis spectrophotometer (Spectronic Instruments Inc., Rochester, NY, USA) and compared to $Fe(NH_4)_2SO_4$ standards.

Total iron (Fe^{2+} and Fe^{3+}) in the extracts was measured by inductively coupled plasma mass spectrometry (ICP-MS) on a Finnigan Mat (Thermo Electron, Bremen, Germany) high resolution ICP-MS using a 10 p.p.b. indium internal standard added to allow correction for fluctuations in the rate of sample uptake and nebulization. Ferric iron was calculated by subtracting ferrous iron measured by UV/Vis from total iron measured by ICP-MS.

Gravimetric moisture content of duplicate regolith samples was determined by oven-drying samples at 105 °C for 24–48 h.

Organic carbon in the saprolite and soil samples was measured by combustion using a CE instruments NC 2500 elemental analyser after HCl extraction of inorganic carbon, which was negligible. Particle size distributions were determined by the hydrometer method (Gee & Bauder, 1986), based on sedimentation rates following Stokes' Law. We used the USDA classification for soil particle sizes, which defines particles 50 to >2000 μm as sand, 2–50 μm as silt, and <2 μm as clay.

Enumeration of total cells and culturable heterotrophs

Samples (~3 g) of soil or saprolite were suspended in 27 mL of 0.1% peptone (Zuberer, 1994). The suspensions were vortexed for 1 min and the coarse particles allowed to settle for 1 min. A portion of the liquid above the coarse particles was fixed immediately with formaldehyde (3.7% final concentration) and stored at 4 °C for subsequent microscopic examination. Another portion of the liquid was serially diluted tenfold in 0.1% peptone for spread-plating of 0.1-mL aliquots on R2A agar plates (Difco, Detroit, MI, USA), an oligotrophic nutrient medium shown to recover higher numbers of stressed cells from environmental samples (Reasoner & Geldreich, 1985). Plates were incubated at 25 °C for 10 days (beginning 8 days after sample collection in the field). Numbers of colonies with morphologies typical of actinobacteria and fungi were also recorded to assess compositional changes in culturable heterotrophs. Numbers of colony-forming-units were reported on the basis of oven-dry weights of regolith. Genomic DNA from four commonly observed colonies obtained from the 4.3-m sample was amplified by polymerase chain reaction with universal bacterial primers (Lane, 1991) to obtain 16S rRNA gene sequences for cloning and BLAST analysis.

Formaldehyde-fixed cell suspensions were diluted further with buffer (0.5 M Na_2HPO_4 and 0.85% NaCl adjusted to pH 9.0) to obtain final dilutions of 1 : 50, 1 : 500, and 1 : 5000. A 5-μL aliquot of each dilution was smeared evenly within a 6-mm diameter well on slides (Cell-Line Associates Inc., Newfield, CA, USA) to obtain smears with different cell densities. After air-drying smears were stained for 30 min with 20 μL DTAF (5-(4,6-dichlorotriazin-2-yl) aminofluorescein) at a concentration of 0.2 mg mL^{-1} buffer. DTAF is a protein stain with binding, absorption, and emission peaks (at 488 and 510 nm, respectively) nearly identical to those of fluorescein isothiocyanate (Sherr *et al.*, 1987). DTAF exhibits less non-specific fluorescence in soil samples than nucleic acid stains such as acridine orange (Bloem *et al.*, 1995; Bruns *et al.*, 1999). Slides were rinsed twice in buffer for 20 min, then in sterile water for a few seconds and allowed to air dry before counting with Nikon Eclipse E600 and Nikon Eclipse i50 fluorescence microscopes at 600× magnification. Smears yielding 10–50 cells per microscope field were selected for counting to reduce error due to cell masking at higher densities (Bloem *et al.*, 1995). Sufficient numbers of microscope fields were inspected to enumerate at least 300 cells per sample, and all counts were obtained by one investigator.

DNA extractions

DNA extractions were performed using a sequential chloroform extraction method, based on Zhou *et al.* (1996), designed to minimize DNA shearing. The DNA extractions were undertaken within 3 weeks after sample collection in the field. Briefly, 10 g soil or saprolite (moist wt) in 50-mL centrifuge tubes was vortexed with 13.5 mL extraction buffer containing 0.1 M potassium phosphate (pH 8.0), 0.1 M EDTA (pH 8.0), 0.1 M Tris-HCl (pH 8.0), and 1.5 M NaCl. After adding 50 μL proteinase K (10 mg mL^{-1}), tubes were shaken horizontally at ~11 g for 30 min at 37 °C. After shaking, 1.5 mL 20% sodium dodecyl sulfate (SDS) was added and samples were incubated in a 65 °C water bath for 2 h, with gentle end-over-end inversions every 20 min. Supernatants were collected after centrifugation at 6000 *g* for 10 min at room temperature and transferred to clean 50-mL tubes. Regolith pellets were extracted two more times by adding 4.5 mL of the extraction buffer and 0.5 mL of 20% SDS, vortexing for 10 s, incubating at 65 °C for 10 min, and centrifuging as before. Supernatants from the three cycles of extractions were combined and mixed with an equal volume of chloroform-isoamyl alcohol (24 : 1 v/v). The aqueous phase was recovered after centrifugation and precipitated with 0.6 volume of isopropanol. Precipitates were collected by centrifugation at 16 000 *g* for 20 min at room temperature, washed with cold 70% ethanol, and resuspended in 200–500 μL 10 mM Tris-HCl. Final purification of 50 μL crude DNA involved processing through the purification steps (from step 13) of the Mo Bio UltraClean™ Soil DNA Isolation Kit. DNA in extracts was quantified by spectrophotometric absorption at 260 nm and purity was assessed from absorbance rations at 260/280 and 260/300 nm using a PerkinElmer Instruments Lambda 40 UV/VIS spectrometer (Bruns & Buckley, 2002).

Biological activity reaction tests

Biological activity reaction tests (BART™), manufactured by Droycon Bioconcepts Inc. (Regina, SK, Canada), were used to detect iron-related bacteria (IRB) in samples from each saprolite depth interval of the 2004 (5 m) core. IRB-BART™ tests results were evaluated according to the manufacturer's instructions. BART™ tests have been used for research applications including the detection of sulfate-reducing bacteria (SRB) in bacterial mats (Pimenov & Ivanova, 2005); evaluation of iodine toxicity to IRB, SRB, and slime-forming bacteria (Sheppard & Hawkins, 1995); and enumeration of IRB and SRB in soil cores to 3.4 m depth (Bhupathiraju *et al.*, 2002). BART™ tests are based on establishing redox gradients in tubes containing growth medium, which permits

organisms with different oxygen requirements to grow at different levels in the medium. The BART™ test vials contain a dried pellet of selective media at the bottom and a floating ball that restricts oxygen supply to the solution below. Oxygen diffuses around the edges of the ball permitting growth of aerobic micro-organisms. As aerobes grow, they quickly use up the oxygen as it diffuses into the solution below the ball. A redox gradient is thus created with oxic conditions at the top and anoxic conditions at the bottom of the test vials. Consequently, aerobic, microaerophilic, and anaerobic micro-organisms can grow in different zones of the test vials.

The IRB-BART™ tests can detect both iron-oxidizing and iron-reducing bacteria as well as pseudomonads, enteric, and heterotrophic bacteria. The IRB-BART™ test media contains ferric ammonium citrate, providing iron, nitrogen, and carbon. Development of foam and/or brown colouration in the vial indicates the presence of anaerobic and/or aerobic IRB, respectively. The composition of the IRB community can be estimated from the observed reaction pattern signatures that are sequences of 1–3 reactions (out of 8 possible) that have been calibrated by the manufacturer. For each sampling depth, 0.5 g of wet soil or saprolite mixed with 15 mL of phosphate buffered saline (PBS) buffer was added to each of BART™ test vials and capped. Vials were stored in the dark at room temperature for 10 days and observed and photographed daily. Control vials were run containing only PBS buffer without sample.

RESULTS

Field observations

For both cores, surface samples were wet, clay-rich, and contained roots and plant material. Between 0.5 and 1.1 m depth, samples became increasingly drier and roots fewer. Roots and plant material were only observed in samples collected from less than 1.1 m depth. Saprolite texture was discernible at 1.2 m and below. Although most of the saprolite has a uniform texture, horizontal linear zones enriched in manganese oxides were visible in the auger bucket at about 2.4, 4.6–4.9 m, and less distinct zones were observed at about 3.8 and 4.1 m (Fig. 2A). Such visible heterogeneities were observed in both cores, although depths of these layers were only recorded in the 5 m (2004) core.

Chemical and physical parameters

Calculations of the mass transfer coefficient for Fe, $\tau_{Zr,Fe}$ (Fig. 2B), indicated no significant trends with distance from the parent rock (or upwards through the profile from the bedrock to the soil) and much variability in the mobility of Fe throughout the profile. In contrast, $\tau_{Zr,Mn}$ indicates a distinct trend of Mn depletion with increasing distance from the parent rock, but with several significant enrichment zones corresponding to depths where Mn oxides were visible before removal from the auger bucket (Fig. 2A).

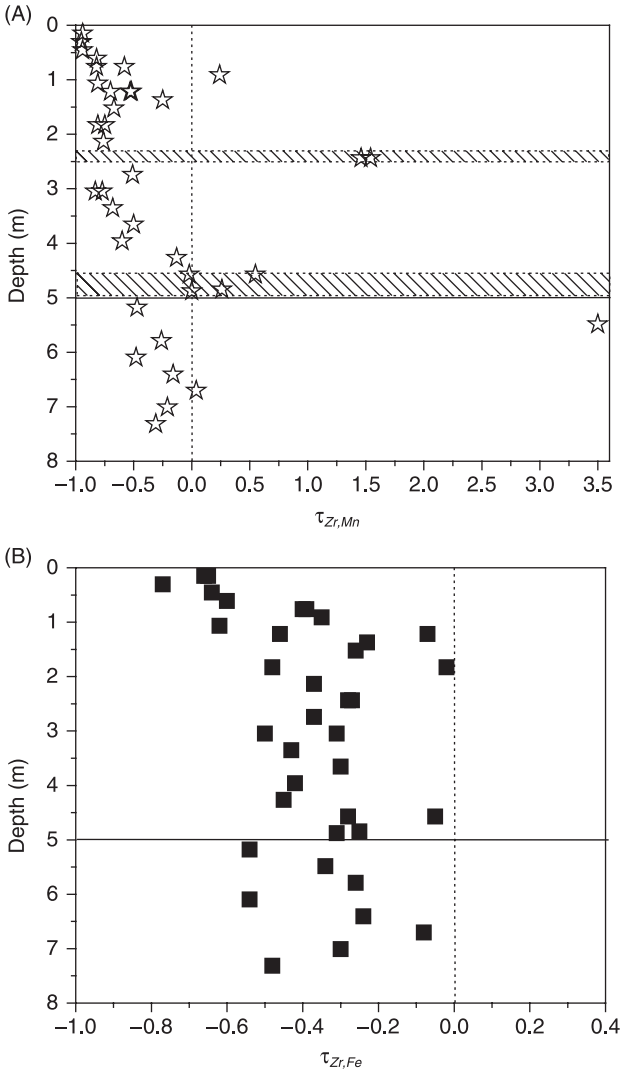

Fig. 2 Mass transfer coefficients ($\tau_{Zr,j}$, loss or gain from the parent rock during weathering) of individual elements *j* relative to Zr calculated for each sample depth (Brimhall & Dietrich, 1987). If $\tau_{Zr,j} = -1$, the element is entirely lost. If $\tau_{Zr,j} > 0$, a net gain of the element relative to the parent rock is indicated. The vertical dashed line at $\tau_{Zr,j} = 0$ indicates no change relative to the parent rock composition. The solid horizontal line at 5 m depth indicates the approximate location of the saprolite-bedrock interface. Data points below this line are for samples taken from the partially weathered, but more cohesive, spheroidal weathering layers (rindlets) that cap the unweathered bedrock and comprise the weathering interface. Bedrock samples were taken from a nearby roadcut because we were unable to penetrate into the least-weathered rindlets and the bedrock with the auger. (A) $\tau_{Zr,Mn}$ reveals zones of Mn enrichment in the saprolite, which were observed in the field at sampling depths indicated by the horizontal hachured zones. (B) $\tau_{Zr,Fe}$ shows much variability with no identifiable trend of depletion or enrichment through the profile.

Concentrations of HCl-extractable Fe(II) and Fe(III) were highest in the top meter of the profile, low and relatively constant from 1 to 4 m depth, and higher at the bottom of the

profile (Table 1, Fig. 3). A slight increase in both Fe(II) and Fe(III) were observed at 2.4 m. Moisture and clay content (Table 1, Fig. 4) were highest in the top meter and relatively constant through the rest of the profile (1–5 m). The silt-sized fraction was lowest (19–26 wt percentage) in the top 0.5 m of the profile, then increased to a variable 30–55 wt percentage down to 5 m depth. The sand-sized fraction accounted for 29–49 wt percentage of the material but showed no significant trends through the profile.

Biological results

Direct microscopic counts of DTAF-stained cells in the upper 0.6 m of soil of the 2003 and 2004 cores ranged from 4.0×10^9 to 1.6×10^{10} g^{-1}. Below 0.6 m cell densities were lower but varied by more than two orders of magnitude (from 2.5×10^6 to 7.9×10^8 cells g^{-1}, Table 2). Cell densities in the upper portion of the profile appeared to follow a pattern similar to that of organic carbon content, as shown by data for the 2003 core (Tables 1 and 2). In the 2004 core, direct counts made at depths between 3.7 and 4.9 m showed higher cell numbers than at intermediate depths and ranged between 1.0×10^8 g^{-1}–1.3×10^9 g^{-1}(Table 2, Fig. 5A). Notable observations from the 2004 core were the increased cell densities at 2.1 m and between 3.7 and 4.9 m depths.

For the 2004 core, counts of culturable cells, based on colony-forming units (CFUs) on R2A plates, ranged from 0.0004 to 0.02% of the total cell numbers estimated by direct microscopy (Table 2, Fig. 5A). One exception to this pattern was observed at 4.6 m depth, where CFUs made up 0.8% of the direct microscopic count. DNA yields ranged from 120 to 52 000 ng DNA g^{-1} oven-dry saprolite or soil. In the upper 1.2 m of the 2004 core, DNA yields exhibited decreases similar to those of total and culturable cell densities (Table 2, Fig. 5B). Between 1.2 and 4.6 m of the 2004 core, DNA yields remained low (between 200 and 600 ng g^{-1} soil or saprolite) but increased to 20 000 ng g^{-1} at 4.9 m. Although this relatively high DNA yield was not observed at precisely the same depth as the highest CFU count (i.e. 7.9×10^6 g^{-1} at 4.6 m), the CFU count of 3.2×10^4 g^{-1} was still higher at 4.9 m than at intermediate depths (Fig. 5A). Higher cell densities and DNA yields therefore provided evidence for greater biomass in the saprolite just above the rindlet zone (at 4.6–4.9 m) in the 2004 core.

Table 1 Chemical and physical measurements for the Guaba ridge saprolite*

Depth (m)	†Moisture (wt %)	‡Particle size distribution			§Organic Carbon (wt %)	¶HCl extractions	
		Sand (wt %)	Silt (wt %)	Clay (wt %)		Total Fe (μmol g^{-1})	Fe^{2+} (μmol g^{-1})
0.15	45.3 ± 0.0	47 ± 5	23 ± 5	30 ± 2	1.62 ± 0.49	70.27 ± 12.3	1.98 ± 0.21
0.30	45.9 ± 0.1	39 ± 5	19 ± 5	42 ± 2	1.45 ± 0.44	69.36 ± 7.72	1.81 ± 0.50
0.46	42.8 ± 0.3	46 ± 5	26 ± 5	28 ± 2	1.19 ± 0.36	58.85 ± 1.43	1.43 ± 0.05
0.61	42.9 ± 3.9	29 ± 5	55 ± 5	16 ± 2	1.11 ± 0.33	54.19 ± 1.59	2.01 ± 0.27
0.76	35.4 ± 0.4	39 ± 5	40 ± 5	21 ± 2	0.18 ± 0.05	22.31 ± 7.49	0.90 ± 0.06
0.91	27.3 ± 0.1	45 ± 5	38 ± 5	17 ± 2	–**	5.23 ± 0.80	0.39 ± 0.03
1.07	26.8 ± 0.6	35 ± 5	42 ± 5	23 ± 2	–	2.45 ± 0.12	0.23 ± 0.02
1.22	27.8 ± 1.0	44 ± 5	35 ± 5	21 ± 2	0.14 ± 0.04	2.05 ± 1.02	0.25 ± 0.01
1.37	27.6 ± 0.3	42 ± 5	34 ± 5	24 ± 2	–	2.75 ± 0.44	0.26 ± 0.01
1.52	28.3 ± 0.2	45 ± 5	37 ± 5	18 ± 2	0.41 ± 0.12	1.83 ± 0.12	0.21 ± 0.05
1.83	28.3 ± 3.2	30 ± 5	49 ± 5	22 ± 2	0.11 ± 0.03	2.47 ± 0.09	0.22 ± 0.02
2.13	27.8 ± 0.5	39 ± 5	36 ± 5	25 ± 2	0.19 ± 0.06	1.69 ± 1.14	0.24 ± 0.03
2.44	30.4 ± 0.3	39 ± 5	35 ± 5	26 ± 2	0.04 ± 0.01	5.07 ± 1.24	0.47 ± 0.07
2.74	28.6 ± 0.4	44 ± 5	31 ± 5	25 ± 2	0.15 ± 0.04	3.64 ± 0.09	0.33 ± 0.03
3.05	26.8 ± 0.7	38 ± 5	44 ± 5	18 ± 2	0.09 ± 0.03	2.98 ± 0.50	0.40 ± 0.02
3.35	28.6 ± 0.0	39 ± 5	37 ± 5	24 ± 2	–	3.41 ± 0.36	0.35 ± 0.09
3.66	29.1 ± 0.2	40 ± 5	40 ± 5	20 ± 2	0.11 ± 0.03	2.98 ± 0.95	0.31 ± 0.03
3.96	31.1 ± 0.0	33 ± 5	46 ± 5	21 ± 2	0.08 ± 0.02	3.31 ± 0.08	0.33 ± 0.01
4.27	32.5 ± 1.5	47 ± 5	32 ± 5	21 ± 2	0.11 ± 0.03	9.76 ± 3.93	0.60 ± 0.02
4.57	34.3 ± 0.2	45 ± 5	36 ± 5	20 ± 2	0.18 ± 0.05	9.25 ± 1.20	0.59 ± 0.04
4.88	28.4 ± 0.4	49 ± 5	30 ± 5	21 ± 2	0.09 ± 0.03	31.93 ± 0.43	0.85 ± 0.02

*All data reported here are for the 2004 regolith core except organic carbon, which was measured on the 2003 core.

†Gravimetric moisture content determined by oven-drying. Error is standard deviation between duplicate samples.

‡Particle sizes determined by the hydrometer method (Gee & Bauder, 1986). Errors given are for methodological uncertainties as described by Gee & Bauder (1979, 1986).

§Organic carbon measured by combustion after HCl extraction of inorganic carbon. Variability among replicate samples is less than 30%, which is used here as a conservative estimate of error. **Extractions were performed in duplicate for each sampling depth and measurements made in triplicate on each extract. Error is the standard deviation between the duplicate samples.

¶Dashes (–) indicate no measurement.

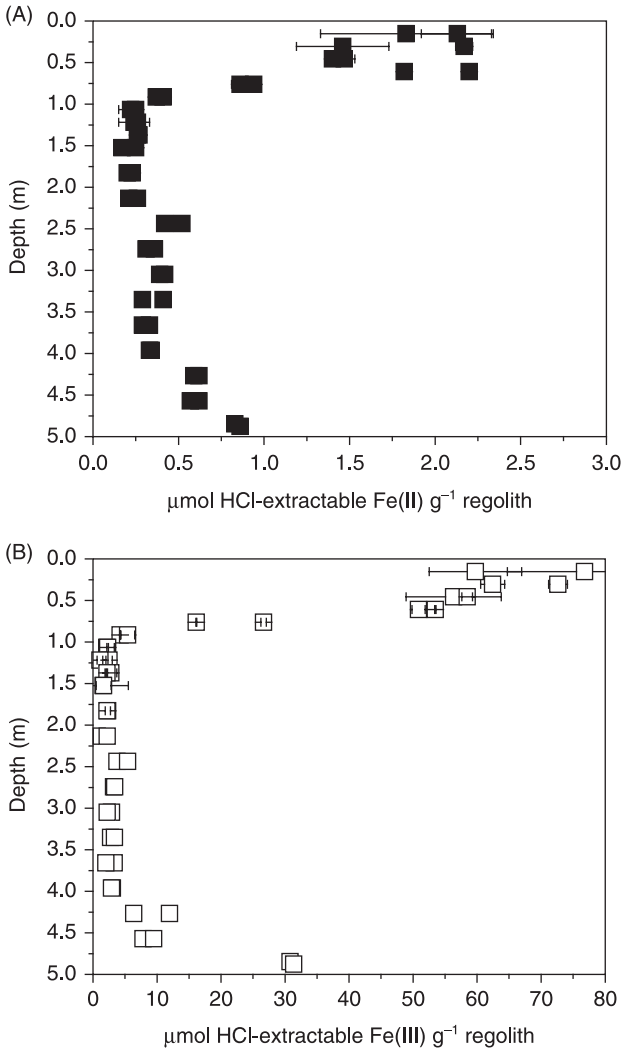

Fig. 3 Iron extracted from saprolite using 0.5 N HCl, plotted vs. depth. (A) Fe(II) in the extracts was measured by UV/Vis spectrophotometry using a standard ferrozine assay (Stookey, 1970; Gibbs, 1976). (B) Fe(III) in the extracts was calculated as the difference between total iron (measured by ICP-MS) and Fe(II).

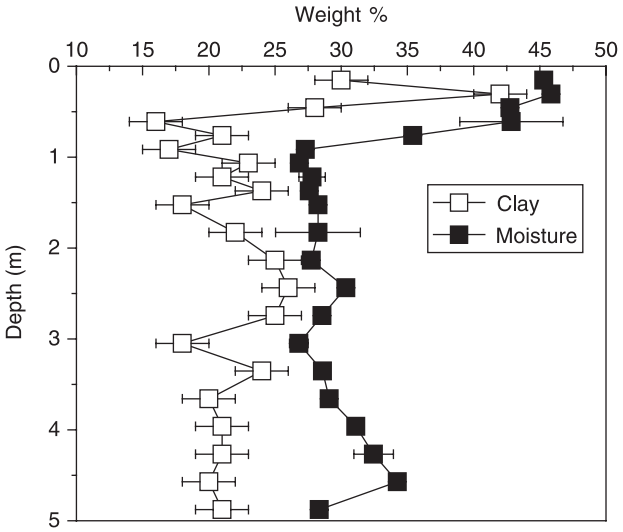

Fig. 4 Clay and moisture content (wt percentage) of the saprolite. Clay is the <2 μm size fraction of the saprolite particles. Particle sizes were measured by the hydrometer method, which is based on sedimentation rates according to Stokes' Law (Gee & Bauder, 1986). Gravimetric moisture content was determined by oven-drying the saprolite samples for 24–48 h and comparing wet and dry weights.

Differences in colony morphologies on R2A plates were noted to evaluate compositional changes in culturable organisms with depth in the 2004 core. At most depths, culturable actinobacteria and fungi were not dominant, except at 1.4 and 1.8 m, where CFU counts were lowest (Table 2, Fig. 5A). For the sample at 4.3-m depth, genomic DNA was obtained from four different colonies with commonly observed morphologies to obtain partial 16S rRNA gene sequences; these were most closely related to the common soil bacteria *Streptomyces griseus, Micromonospora* sp., and *Bacillus subtilis*. Some of the culturable organisms from the sample at 4.6-m depth produced in the R2A medium a diffusible yellow-green fluorescent pigment, which is characteristic of pseudomonads. This pigment was not observed in plates from any other depth. Interestingly, this sample also had the highest CFU g^{-1} in the entire profile. The presence of culturable fluorescent pigment producers was unique to this sample and provided a clear indication of bacterial community differences at this depth.

All IRB-BART^{TM} tests turned cloudy within 2 days, indicating general heterotrophic activity. A brown gel formed at the bottom of some sample tubes after day 4 indicating a mixed community of heterotrophs and iron-oxidizing bacteria (IOB) with some enteric bacteria (Droycon Bioconcepts Inc., 2003). This positive result for IOB occurred in samples from the uppermost section of the profile (0.15–0.6 m), the middle of the profile (2.1 and 2.4 m, coincident with the spike in the direct count cell numbers) and the bottom of the profile (4.9 m).

DISCUSSION

Geomicrobiology of the regolith

At depth near the saprolite–bedrock interface, increases were seen in densities of total cells, culturable cells, and iron-oxidizing bacteria, as well as in HCl-extractable iron (Figs 3 and 5). HCl-extractable Fe(II) shows the highest coefficient of determination ($r^2 = 0.56$, $P = 0.0002$) with respect to cell numbers of all of the parameters measured (Fig. 6). The similar trends for concentrations of 'bioavailable' iron, cells, and iron-oxidizing bacteria may be consistent with either (i) a population of saprolite bacteria that varies as a function of available iron in the saprolite, or (ii) a population of bacteria that *causes* the increased bioavailable iron.

Table 2 Biological data from the Guaba ridge regolith profile

	*Direct count log(cells g^{-1})			% CFU				
Depth in m	2003 core	2004 core	†Total CFU log (CFU g^{-1})	(neither actinobacteria or fungi)	(w/typical actinobacterial morphology)	(w/typical fungal morphology)	‡DNA log (ng g^{-1})	§IRB-BART™ (+/–)
0.15	10.2	–¶	5.7	100	<0	<0	–	+
0.30	10.1	9.8	5.5	100	<0	<0	4.7	+
0.46	10.1	9.6	5.5	100	<0	<0	4.7	+
0.61	9.6	9.7	5.2	88	6	6	4.3	+
0.76	8.8	8.5	4.8	100	<0	<0	3.8	–
0.91	–	8.4	4.3	66	34	<0	2.6	–
1.07	–	8.0	3.6	75	25	<0	2.8	–
1.22	8.7	7.2	1.8	100	<0	<0	2.4	–
1.37	–	7.6	3.8	40	40	20	<2	–
1.52	8.5	7.5	3.3	66	34	<0	<2	–
1.83	8.3	6.4	2.1	<0	50	50	<2	–
2.13	8.5	8.9	3.5	70	20	10	2.4	+
2.44	7.5	7.3	2.7	100	<0	<0	<2	+
2.74	7.3	–	3.4	70	30	<0	<2	–
3.05	–	7.3	2.9	60	20	20	<2	–
3.35	–	6.9	3.1	75	15	10	<2	–
3.66	–	8.0	2.9	80	8	12	<2	–
3.96	–	8.4	3.7	80	20	<0	2.8	–
4.27	–	9.1	3.8	90	8	2	2.5	–
4.57	–	9.0	6.9	100	<0	<0	<2	–
4.88	–	8.4	4.5	100	<0	<0	4.3	+

*Direct counts were performed on DTAF-stained samples examined by epifluorescence microscopy. Detection limit for microscopic counts was assumed to be *c.* 10^7 cells g^{-1} oven-dry regolith (soil or saprolite).

†Plate counts of colony-forming units (CFUs) g^{-1} oven-dry regolith performed on R2A agar plates incubated at 25 °C for 10 days. Separate counts of colonies with characteristic morphologies for actinobacteria and fungi were tracked and reported as percentages of total CFUs.

‡DNA concentration was measured by absorbance at 260 nm.

§IRB-BART™ = biological activity reaction test for iron related bacteria performed on regolith samples collected in 2004.

¶No measurement indicated by dashes (–).

The two zones of visible manganese enrichment at 2.4 and 4.6–4.9 m coincided with relatively higher cell numbers, Mn oxide concentrations and values of $\tau_{Zr,Mn}$, presence of iron-oxidizing bacteria, and concentrations of HCl-extracted Fe(II) and Fe(III). The 4.6–4.9 m samples were nearest the saprolite–bedrock interface. The 2.4 m zone probably represents a zone of 'ghost rindlets'; in other outcrops elsewhere in the Rio Icacos watershed we have observed these highly weathered rindlets detached from the bedrock corestone and surrounded by saprolite. These are interpreted as saprolite grains that retain the visible features and chemistry of bedrock rindlets. For example, the 2.4 m zone coincided with the previously reported increase in the Fe^{2+}/Fe^{3+} ratio (Murphy, 1995) in mica grains. Mn is a constituent of the biotite grains in the saprolite, rindlets, and bedrock (0.1–0.6 wt percentage MnO in biotite, Murphy, 1995) and of the hornblende grains in the rindlets and bedrock (0.6–1.2 wt percentage MnO in hornblende, data not shown). These less weathered ghost rindlets therefore are interpreted to retain both the visible features of bedrock rindlets as well as the less-weathered biotites that provide a source of reduced metals for microbial life at 2.4 m depth.

Chemical weathering controls on biomass

Microbial ecologists have long recognized that 1% or less of all micro-organisms in environmental samples are culturable (Hugenholtz *et al.*, 1998). Thus, it is difficult to quantify populations with specific functions (e.g., iron oxidation) in uncharacterized microbial communities. In this section we present a model using substrate fluxes to estimate growth rates of the active iron-oxidizing and heterotrophic populations in the deep saprolite just above the saprolite–bedrock interface.

Researchers including Brown *et al.* (1995), Heimsath *et al.* (1999), and von Blanckenburg *et al.* (2004) have previously assumed that soils developed on granite, sandstone, and metamorphosed crystalline bedrock are steady state in thickness. Riebe *et al.* (2003) and Brown *et al.* (1995) propose that the regolith profiles in Rio Icacos are undergoing steady state regolith (soil + saprolite) formation, erosion, and weathering such that the total mass of the regolith in the watershed is approximately constant through time. Conservation of mass implies that the rate of regolith formation from parent material is equal to the total denudation rate, which in turn is equal to

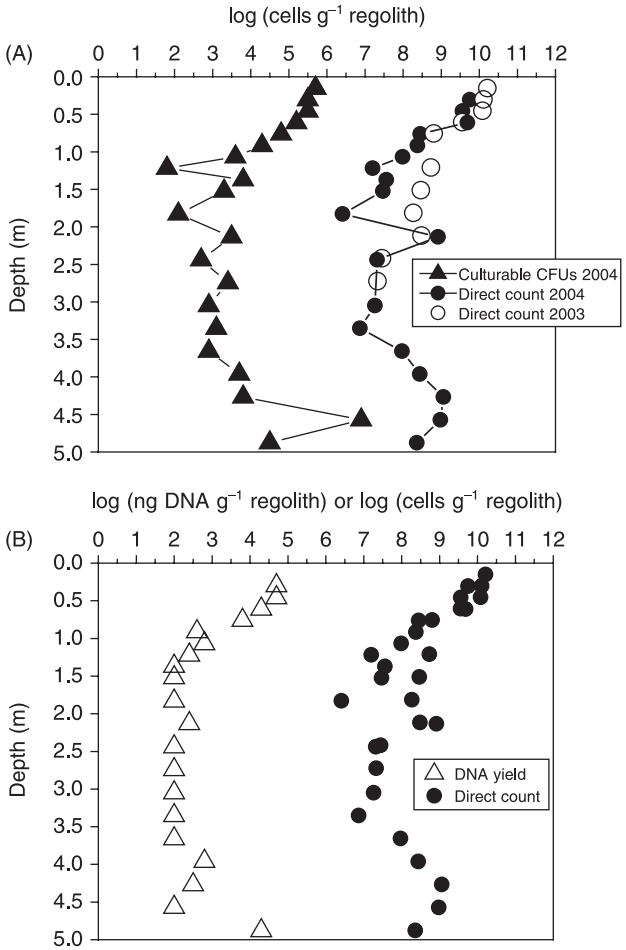

Fig. 5 (A) Cells were directly counted in the 2003 (0.15–2.7 m depth) and 2004 (0.15–5.0 m depth) saprolite cores using fluorescent microscopy after staining with DTAF. Sufficient numbers of microscope fields (containing 10–50 cells each) were inspected to count at least 300 cells per sample, and all counts were obtained by one investigator. Plate counts of colony-forming units (CFUs) in log (CFU g^{-1} regolith) were performed on R2A agar plates. (B) Comparison of direct counts (which here include data points from both 2003 and 2004) to DNA yield in log (ng DNA g^{-1} regolith). Cell counts and DNA yields are given in terms of regolith dry weight.

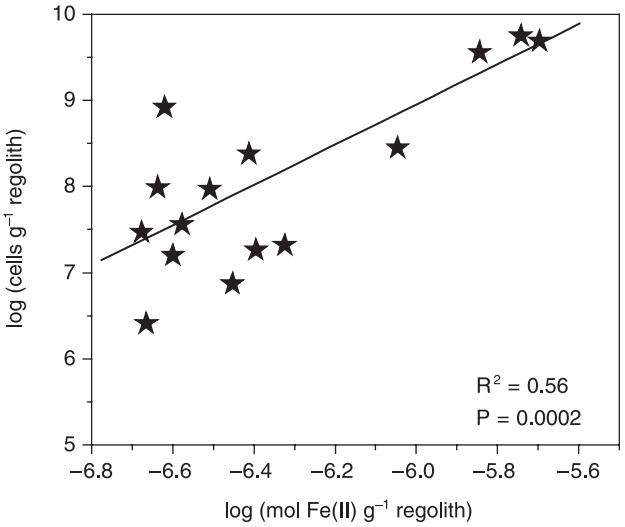

Fig. 6. A linear regression between direct cell counts in log cells g^{-1} regolith vs. HCl-extracted Fe(II) in µmol g^{-1} regolith reveal a relationship between cell numbers and Fe(II).

the sum of the rates of chemical weathering and physical erosion. Riebe *et al.* (2003) generally assume that elemental soil profiles (element concentration vs. depth) are steady state as well. Calculated weathering rates based on soil denudation (Brown *et al.*, 1995; Riebe *et al.*, 2003) agree with weathering rates based on advance of the saprolite-bedrock interface (White *et al.*, 1998) supporting the steady state assumption. In a steady state weathering profile, the value for a property at a given depth remains constant as a function of time, because of the assumed balance in production and loss of particles through weathering and erosion, respectively. Fletcher *et al.* (in press) proposed that the weathering advance rate for the Rio Icacos quartz diorite – the rate that the bedrock transforms to saprolite – is controlled by the chemistry of pore fluids at depth and that this chemistry is in turn controlled by the thickness of the saprolite profile.

While the concept of steady state has been proposed for soils and saprolites, little to no work has been completed to investigate the idea of a steady state biomass profile. We discuss here a model that assumes that the profiles of yearly averaged cell biomass and organic carbon as a function of depth are constant with time. We also assume in the model that the depth profiles of iron-oxidizing and heterotrophic bacterial mass vs. depth are invariant. Because the regolith studied here is positioned on a knife-edge ridge, downward-moving pore fluid will flow laterally when it reaches the bedrock–saprolite interface. Although the hydrologic system is therefore inherently 2D, for simplicity we only consider 1D vertical flow. Thus, in this discussion we implicitly assume that pore fluid flows through both the saprolite and the bedrock, but fluid only reacts chemically with the saprolite and not with the bedrock. In effect, the lateral flow is incorporated within our model as chemically nonreactive vertical flow through the bedrock. Although this assumption is unrealistic, it enables simplification for allowing a preliminary step in interpretation of biomass within a steady state profile. We further restrict ourselves to consideration only of the saprolite profile, ignoring the soil profile above 1 m.

From the perspective of the biomass at the saprolite–bedrock interface, and ignoring other inorganic substrates that are presumably present at insignificant concentrations, metabolizable substrate is delivered as a mass flux of dissolved organic carbon or dissolved Fe(II). The flux of Fe(II) is delivered by solubilization of bedrock. This latter solubilization, when considered through the perspective of a unit of immobile

biomass at the saprolite–bedrock interface, delivers a slow but steady concentration of aqueous Fe(II) as the rindlet zone advances into intact bedrock over time.

Variations of properties (e.g. substrate concentrations) with depth can be described using either of two different frames of reference (Berner, 1980): with respect to a fixed layer or a fixed depth. If properties are expressed in terms of a fixed layer origin, the origin moves upward as the profile moves downward due to weathering and erosion. In the case of a fixed depth origin (e.g. the saprolite–bedrock interface), the origin moves downward at the same rate as the rest of the profile. In a steady state profile with a fixed depth origin, the value of a property in a given layer will vary with time, but the property at a given depth will remain constant. Here we choose the fixed depth frame of reference taking as our origin the saprolite–bedrock interface; we express mass balance of component i in an infinitely thin layer of saprolite at this origin:

$$\frac{\partial C_i}{\partial t} = -\frac{\partial F_i}{\partial x} + \sum R_i \qquad (3)$$

Here C_i is the concentration of component i (mol m^{-3} saprolite); F_i is the flux of component i into or out of the layer of saprolite (mol m^{-2} saprolite h^{-1}); and R_i refers to the reactions that release or consume component i to or from the saprolite (mol m^{-3} saprolite h^{-1}) (Berner, 1980). Variables x and t refer to distance increasing upward from the saprolite-bedrock interface and time, respectively. Note that weathering of bedrock to saprolite at Rio Icacos is isovolumetric (White *et al.*, 1998), so the layer experiences no volume change as the profile evolves.

In rindlets where porosity is very low (<0.1%) and transport is diffusion-controlled, abiotic oxidation of Fe(II) is hypothesized to form Fe(III)-oxide precipitates that crack the rock (Fletcher *et al.*, in press). It is reasonable to suppose that the bedrock and rindlets are therefore dominated by abiological iron-oxidation. Presumably, bacterial iron-oxidation controls the Fe(II) oxidation rate in the saprolite but not in the rindlets because in the saprolite the abiological processes have disaggregated the rock to the extent that advection dominates transport. Therefore to model fluxes in the saprolite just above the rindlets, we assume that the advective flux is dominant over the diffusive flux where v is the rate of advective transport (m h^{-1}):

$$F_i = v C_i \qquad (4)$$

For simplicity, we assume that the source of Fe(II) from bedrock is due to weathering of hornblende, which disappears within the rindlet zone (White *et al.*, 1998; Buss *et al.*, 2004) as the bedrock weathers isovolumetrically to saprolite. The HCl-extractable Fe(II) in the deepest saprolite represents the Fe(II) released from hornblende as the rindlets transform to saprolite. Biotite weathering also releases Fe(II) (Murphy *et al.*, 1998) but we ignore this flux since biotite persists throughout the saprolite profile and thus, cannot be the controlling feature causing rindlet formation and disaggregation.

As a first approximation, we assume that the dominant sink for Fe(II) within the deep saprolite is oxidation by Fe-oxidizing bacteria. Thus, the rate of change of Fe(II) in the volume of saprolite at the saprolite–bedrock interface can be expressed as:

$$\frac{\partial(C_{Fe(II)})}{\partial t} = -\frac{\partial(vC^{aq}_{Fe(II)})}{\partial x} - \frac{\partial(\omega C^{rz}_{Fe(II)})}{\partial x} - \frac{\beta_{IOB}}{\Upsilon_{Fe(II)}} \qquad (5)$$

where β_{IOB} (mol C m^{-3} h^{-1}) is the maximum rate of production of iron-oxidizing biomass, $\Upsilon_{Fe(II)}$ is the yield of IOB biomass (mol C biomass mol^{-1} Fe(II) oxidized), ω is the weathering advance rate (m h^{-1}), $C^{aq}_{Fe(II)}$ is the concentration of Fe(II) in pore fluid in the saprolite (mol m^{-3}), and $C^{rz}_{Fe(II)}$ is the concentration of hornblende-incorporated Fe(II) per unit volume of rock in the outermost rindlet (mol m^{-3}) or the concentration of extractable Fe(II) in the deepest saprolite (mol m^{-3}). If the advective flux and ω are constants, then we can write:

$$\frac{\partial(C_{Fe(II)})}{\partial t} = -v\frac{\partial(C^{aq}_{Fe(II)})}{\partial x} - \omega\frac{\partial(C^{rz}_{Fe(II)})}{\partial x} - \frac{\beta_{IOB}}{\Upsilon_{Fe(II)}} \qquad (6)$$

Next we make the steady state assumption on Fe(II) concentration in the layer as a function of time: $\frac{\partial(C^{rz}_{Fe(II)})}{\partial x} = 0$. Based on the rate of advance of the saprolite–bedrock interface due to weathering, ω, we calculate a rate of production of iron-oxidizing biomass:

$$\beta_{IOB} = \Upsilon_{Fe(II)}\left[-v\frac{\partial(C^{aq}_{Fe(II)})}{\partial x} - \omega\frac{\partial(C^{rz}_{Fe(II)})}{\partial x}\right] \qquad (7)$$

Equation 7 expresses the rate of growth of biomass, β_{IOB}, as a function of the weathering advance rate and the advective flux of Fe(II). Because we are assuming constant ω, v, $\Upsilon_{Fe(II)}$, and Fe(II) concentration gradients, this implies that β_{IOB} is also constant with time.

The value of $\frac{\partial(C^{rz}_{Fe(II)})}{\partial x}$ can be estimated as the rate of change in Fe(II) across the 2-cm thickness of the outermost rindlet: this concentration varies from 1480 mol Fe(II) m^{-3} rock within the hornblende in the outermost rindlet (Turner *et al.*, 2003) to 6.0×10^{-7} mol extractable Fe(II) m^{-3} saprolite in the lowermost saprolite (Table 1). Using ω = ~100 m Ma^{-1} based on cosmogenic isotopes (Brown *et al.*, 1995; White *et al.*, 1998) yields -8.4×10^{-4} mol Fe(II) m^{-3} h^{-1} for the second term in Equation 6. Setting the advective transport velocity, v, to equal the velocity of water movement through the saprolite, -6.84×10^{-5} m h^{-1} (Schulz & White, 1999) and setting the gradient in $C^{aq}_{Fe(II)}$ to equal the change in iron concentration

in the saprolite pore water with depth (0 μM at 1.2 m and 0.3 μM at 8.5 m, White *et al.*, 1998) we calculate that the first term in Equation 6 (3.1×10^{-10} mol Fe(II) m^{-3} h^{-1}) is negligible compared to the second term; therefore the volumetric flux of Fe(II) substrate that is available for IOB production is equivalent to the second term in Equation 6:

$$\beta_{IOB} = -\Upsilon_{Fe(II)}\omega\frac{\partial(C^{rz}_{Fe(II)})}{\partial x}. \quad (8)$$

To estimate the value of β_{IOB}, we need a value for $\Upsilon_{Fe(II)}$: the only published measurements of such a parameter for non-acidophilic iron-oxidizing bacteria range from 0.3 to 0.7 mol C mol^{-1} Fe(II) calculated for freshwater iron-oxidizing bacteria (Neubauer *et al.*, 2002; Sobolev & Roden, 2004). Here we choose the lowest value: 0.3 mol C mol^{-1} Fe(II) for $\Upsilon_{Fe(II)}$ for iron-oxidation in the deep saprolite. For this value for $\Upsilon_{Fe(II)}$, the maximum rate of growth of iron-oxidizing bacteria for the steady state model is 2.5×10^{-4} mol C m^{-3} h^{-1} (Equation 8).

Similarly we can consider a mass balance on total organic carbon, C_C, in the same volume of saprolite at the saprolite–bedrock interface. The inputs of organic carbon to this saprolite volume are the advective flux of dissolved organic carbon, DOC, from the surface and fixation of organic carbon by autotrophs. Losses of organic carbon from this volume of saprolite are the release of CO_2 during respiration by heterotrophs and the flux of insoluble (or otherwise unrecycled) organic carbon that leaves the saprolite layer as the profile moves downward. Mass balance can be written as:

$$\frac{\partial(C_C)}{\partial t} = \beta_{IOB} - v\frac{\partial(C^{aq}_C)}{\partial x} - \frac{\beta_H}{\Upsilon_C} - \omega\frac{\partial(C^{in}_C)}{\partial x}, \quad (9)$$

where C^{in}_C refers to the concentration of insoluble organic carbon and C^{aq}_C is the concentration of DOC. Here β_H is the growth rate of heterotrophic biomass (mol C m^{-3} h^{-1}), Υ_C is the growth yield of heterotrophic biomass (mol C biomass mol^{-1} C substrate), and $\frac{\partial(C^{in}_C)}{\partial x}$ is the gradient in solid organic carbon in the saprolite (1.2–4.9 m depth, Table 1). At steady state, the rate of change of total organic carbon is zero and we can write:

$$\frac{\beta_H}{\Upsilon_C} = \beta_{IOB} - v\frac{\partial(C^{aq}_C)}{\partial x} - \omega\frac{\partial(C^{in}_C)}{\partial x} \quad (10)$$

Equation 10 indicates that the rate that heterotrophs oxidize organic carbon, releasing CO_2 (β_H/Υ_C) is equal to the difference between the rate that autotrophs fix CO_2 (β_{IOB}) and the net aqueous (input) and insoluble (output) organic carbon fluxes. If the net aqueous + insoluble flux is equal and opposite the rate of autotrophic carbon fixation (β_{IOB}) then no carbon is available for heterotrophic growth and the entire biomass at depth in the saprolite is lithoautotrophic. If the net aqueous + insoluble flux is much smaller than β_{IOB} then the lithoautotrophic growth rate outpaces the heterotrophic growth rate.

The small gradient in organic carbon yields 1.6×10^{-10} mol C m^{-3} h^{-1} for the insoluble flux (the last term in Equation 10), which is insignificant compared to the first term ($\beta_{IOB} = 2.5 \times 10^{-4}$ mol C m^{-3} h^{-1}, Equation 8). The concentration of DOC in the Guaba ridge lysimeters was measured at 208 μM at 0.15 m depth and 125 μM at 6.7 m depth (Murphy, 1995), yielding an estimate of -2.8×10^{-7} mol C m^{-3} h^{-1} for the aqueous flux (the second term in Equation 10), which is also insignificant relative to β_{IOB}. Therefore the dominant flux of organic carbon to the deep saprolite is via carbon fixation by lithoautotrophs. For the organic carbon mass balance (Equation 9) β_{IOB} is actually the rate of growth and death of all lithoautotrophs, which we assume here to be dominated by iron-oxidizing bacteria.

For aerobic heterotrophs, Υ_C can vary from ~0.01–0.8 mol C biomass mol^{-1} C substrate (Heijnen & van Dijken, 1991). This range can be narrowed for aerobic heterotrophs in soils to ~0.3–0.6 mol C biomass mol^{-1} C substrate (Frey *et al.*, 2001). Solving Equation 10 for β_H using 0.5 as a first estimate for Υ_C, we find that the rate of growth of heterotrophic biomass is 1.25×10^{-4} mol C m^{-3} h^{-1}. Substituting Equation 8 into Equation 10 (omitting the insignificant aqueous and insoluble carbon fluxes) demonstrates that rock weathering drives organic carbon and biomass production in the deep saprolite:

$$\frac{\beta_H}{\Upsilon_C} = -\Upsilon_C\Upsilon_{Fe(II)}\omega\frac{\partial(C^{rz}_{Fe(II)})}{\partial x} \quad (11)$$

To test the consistency of these growth rates with literature observations, we estimate biomass yields by dividing the calculated growth rates β_{IOB} or β_H (Equations 8 or 11) by a specific growth rate constant μ (h^{-1}). These constants range from ~0.01–0.3 h^{-1} for bacteria in nonagricultural soils (Barros *et al.*, 2001; Núñez-Regueira *et al.*, 2002; Zelenev *et al.*, 2005). Converting units using the deep saprolite density (1.2×10^6 g m^{-3}) and estimating 3.6×10^{-14} mol C $cell^{-1}$, this range of ‘ gives cell densities on the order of 10^4–10^5 cells g^{-1}. When compared to our total cell count (which includes all visible cells: active, inactive, and dead) at depth in the saprolite of $10^{8.4}$ (Table 2), we see that the calculated growth rates are reasonable.

Despite the broad assumptions made for these calculations, it is apparent that the substrate fluxes at the saprolite-bedrock interface will allow a greater growth rate of IOB than of heterotrophic bacteria. Thus, iron-oxidizing bacteria are likely dominant in the deep saprolite as has been observed in acidic carbon-limited systems (López-Archilla *et al.*, 2001; Rohwerder *et al.*, 2003). Production of organic carbon by autotrophic iron-oxidizing bacteria is the primary source of substrate for heterotrophic bacteria, creating a synergistic community of lithoautotrophs and heterotrophs that is dependent on bedrock weathering. Moreover, by consuming Fe(II) and O_2, iron-oxidizing bacteria alter the concentration gradients of these elements and therefore may

be important in the disaggregation of the bedrock, which is driven by diffusion of O_2 into the bedrock and oxidation of ferrous minerals (Fletcher *et al.*, in press).

Our model calculations show that the substrate flux at the saprolite–bedrock interface is dominated by Fe(II), suggesting that the biota transforms from a heterotrophy-based ecosystem at the top of the profile in the soil, to a lithoautotrophy-based ecosystem at depth. The topsoil biota is presumably controlled by the rate of production of DOC (heterotrophic growth) while the deep saprolite biota is controlled by the rate of release of Fe(II) from disaggregating and solubilizing bedrock through spheroidal weathering (lithoautotrophic growth). While we have not proven that the Fe-oxidizing biota at the bedrock–saprolite interface are driving Fe(II) oxidation and spheroidal weathering of the bedrock, our model is consistent with coupling between the physical and chemical and biological weathering of the quartz diorite through the cycling of Fe(II) at the saprolite–bedrock interface.

CONCLUSIONS

Micro-organisms in the ~5 meters of saprolite in the Rio Icacos watershed respond to the availability of iron as a function of depth. As bedrock weathers, ferrous iron is released from silicate minerals, providing substrate for iron-oxidizing bacteria. In turn, autotrophic iron-oxidizing bacteria fix CO_2, providing organic carbon substrate for other organisms in the ecosystem. In this way, Earth's rock weathering engine drives biomass production at depth in this system. Lithoautotrophs, specifically iron-oxidizing bacteria, may be dominant at depth in the saprolite because they are more favoured by substrate fluxes than heterotrophs. Furthermore, iron-oxidizing bacteria affect the concentrations of dissolved Fe(II) and O_2 and therefore may contribute to disaggregation of the intact bedrock through spheroidal weathering. Such weathering has been attributed to diffusion of O_2 into the bedrock, oxidation of ferrous minerals, and creation of spheroidal fractures around corestones (Fletcher *et al.*, in press). Our results indicate that the activities of bacteria may be important factors in geochemical processes in regolith material below the rooting zone. Efforts are ongoing to develop molecular techniques to obtain better quantitative data for microbial populations. These data will be compared to predictions made by the proposed regolith weathering model, which will be further modified to incorporate.

Definitions of variables

$\tau_{Zr,i}$	Mass transfer coefficient (dimensionless)
ρ_w	Density of weathered material (g m^{-3})
ρ_p	Density of parent material (g m^{-3})
$\varepsilon_{Zr,w}$	Volumetric strain of Zr in weathered material (dimensionless)
$C_{j,w}$	Concentration of element j in weathered material (wt %)
$C_{j,p}$	Concentration of element j in parent material (wt %)
C_i	Concentration of component i per volume of solid (mol m^{-3})
F_i	Flux of component i (mol m^{-2} h^{-1})
R_i	Reaction terms for reactions involving i (mol m^{-3} h^{-1})
ω	Rate of weathering advance of saprolite-bedrock interface (m h^{-1})
v	Rate of advection (m h^{-1})
$C_{Fe(II)}$	Concentration of Fe(II) per volume of solid (mol m^{-3})
C_C^{aq}	Concentration of aqueous organic carbon per volume of solid (mol m^{-3})
$C_{Fe(II)}^{rz}$	Concentration of hornblende-bound Fe(II) in rindlet per volume of solid (mol m^{-3})
$C_{Fe(II)}^{aq}$	Concentration of Fe(II) in pore water per volume of solid (mol m^{-3})
C_C	Concentration of total organic carbon per volume of solid (mol m^{-3})
C_C^{in}	Concentration of insoluble (or otherwise unrecycled) organic carbon per volume of solid (mol m^{-3})
β_{IOB}	Rate of production of iron-oxidizing biomass (mol m^{-3} h^{-1})
β_H	Rate of production of heterotrophic biomass (mol m^{-3} h^{-1})
$Y_{Fe(II)}$	Growth yield of iron-oxidizing biomass (mol mol^{-1})
Y_C	Growth yield of heterotrophs (mol mol^{-1})
μ	Specific growth rate constant (h^{-1})

ACKNOWLEDGEMENTS

We thank J. Troester, A. White, D. Mericle, and R. Fletcher for field support; J. Kittleson for analytical assistance; S. Campos, G. Fillipeli, A. Fink, and S. Christy for laboratory assistance; and Jan Amend and three anonymous reviewers. Funding provided by the Penn State Biogeochemical Research Initiative for Education (BRIE, NSF-IGERT grant DGE-9972759), DOE grant DE-FG02-05ER15675, and the Penn State Center for Environmental Chemistry and Geochemistry. S.L. Brantley acknowledges support from the Center for Environmental Kinetics Analysis supported by the National Science Foundation under grant no. CHE-0431328. H.L. Buss acknowledges fellowship support of the NSF Graduate Research Fellowship Program.

REFERENCES

Amy PS, Haldeman DL (1997) *The Microbiology of the Terrestrial Deep Subsurface*. CRC Press, Boca Raton, FL, pp. 356.

Barros N, Feijóo S, Simoni A, Critter SAM, Airoldi C (2001) Interpretation of the metabolic enthalpy change, ΔH_{met}, calculated for microbial growth reactions in soils. *Journal of Thermal Analysis and Calorimetry* **63**, 577–588.

Berner RA (1980) *Early Diagenesis: A Theoretical Approach*. Princeton University Press, Princeton, NJ.

Bhupathiraju VK, Krauter P, Holman H-YN, Conrad ME, Daley PF, Templeton AS, Hunt JR, Hernandez M, Alvarez-Cohen L (2002) Assessment of *in-situ* bioremediation at a refinery waste-contaminated site and an aviation gasoline contaminated site. *Biodegradation* **13**, 79–90.

Bloem J, Bolhuis PR, Veninga MR, Wieringa J (1995) Microscopic methods for counting bacteria and fungi in soil. In *Methods in Applied Soil Microbiology and Biochemistry* (eds Alef K, Nannipieri P). Academic Press, London, pp. 162–173.

Brimhall G, Dietrich WE (1987) Constitutive mass balance relations between chemical composition, volume, density, porosity, and strain in metasomatic hydrochemical systems: results on weathering and pedogenisis. *Geochimica et Cosmochimica Acta* **51**, 567–587.

Brown ET, Stallard R, Larsen MC, Raisbeck GM, Yiou F (1995) Denudation rates determined from the accumulation of in situ-produced ^{10}Be in the Luquillo Experimental Forest, Puerto Rico. *Earth and Planetary Science Letters* **129**, 193–202.

Bruns MA, Buckley DH (2002) Isolation and purification of microbial community nucleic acids from environmental samples. In: *Manual of Environmental Microbiology* (ed. Hurst CJ), ASM Press, Washington DC, pp. 564–572.

Bruns MA, Stephen JR, Kowalchuk GA, Prosser JI, Paul EA (1999) Comparative diversity of ammonia oxidizer 16S rRNA gene sequences in native, tilled, and successional soils. *Applied and Environmental Microbiology* **65**, 2994–3000.

Buss HL, Sak PB, White AF, Brantley SL (2004) Mineral dissolution at the granite-saprolite interface. *11th International Symposium on Water–Rock Interaction*, Taylor & Francis, Lisse, Netherlands, 819–823.

Castillo-Gonzalez H, Bruns MA (2005) Dissimilatory iron reduction and odor indicator abatement by biofilm communities in swine manure microcosms. *Applied and Environmental Microbiology* **71**, 4972–4978.

Chadwick OA, Brimhall GH, Hendricks DM (1990) From black box to a grey box: a mass balance interpretation of pedogenesis. *Geomorphology* **3**, 369–390.

Droycon Bioconcepts Inc. (2003) *Biological Activity Reaction Test BART™ User Manual*. Droycon Bioconcepts Inc., Saskatchewan, Canada.

Emerson D (2002) Microbial oxidation of Fe(II) and Mn(II) at circumneutral pH. In *Environmental Microbe–Metal Interactions* (ed. Lovely DR). ASM, Washington DC.

Fierer N, Schimel JP, Holden PA (2003) Variations in microbial community composition through two soil depth profiles. *Soil Biology and Biochemistry* **35**, 167–176.

Fletcher RC, Buss HL, Brantley SL (2006) Physical–chemical feedbacks between atmospheric oxygen and bedrock weathering during steady-state spheroidal weathering. *Earth and Planetary Science Letters* in press.

Fredrickson JK, Fletcher M (2001) *Subsurface Microbiology and Biochemistry*. Wiley-Liss, pp. 341.

Frey SD, Gupta VVSR, Elliott ET, Paustian K (2001) Protozoan grazing affects estimates of carbon utilization efficiency of the soil microbial community. *Soil Biology and Biochemistry* **33**, 1759–1768.

Gee GW, Bauder JW (1979) Particle size analysis by hydrometer: a simplified method for routine textural analysis and a sensitivity test of measurement parameters. *Soil Science Society of America Journal* **43**, 1004–1007.

Gee GW, Bauder JW (1986) Particle-size analysis. In *Methods of Soil Analysis, Part I. Physical and Mineralogical Methods*. American Society of Agronomy – Soil Science Society of America, Madison, WI, pp. 383–411.

Gibbs CR (1976) Characterization and application of FerroZine iron reagent as a ferrous iron indicator. *Analytical Chemistry* **48**, 1197–1201.

Hallbeck L, Pedersen K (1991) Autotrophic and mixotrophic growth of *Gallionella ferruginea*. *Journal of General Microbiology* **137**, 2657–2661.

Heijnen JJ, van Dijken JP (1991) In search of a thermodynamic description of biomass yields for the chemotrophic growth of microorganisms. *Biotechnology and Bioengineering* **39**, 833–858.

Heimsath AM, Dietrich WE, Nishiizumi K, Finkel RC (1999) Cosmogenic nuclides, topography, and the spatial variation of soil depth. *Geomorphology* **27**, 151–172.

Holt JG, Krieg NR, Sneath PHA, Staley JT, Williams ST (1994) *Bergey's Manual of Determinative Bacteriology*. Williams & Wilkins, Baltimore, MD, pp. 787.

Hugenholtz P, Goebel BM, Pace NR (1998) Impact of culture-independent studies on the emerging phylogenetic view of bacterial diversity. *Journal of Bacteriology* **180**, 4765–4774 (Erratum 180: 6793).

Kurtz AC, Derry LA (2004) Tracing silicate weathering and terrestrial silica cycling with Ge/Si ratios. *The 11th International Symposium on Water–Rock Interaction*, Taylor & Francis, Lisse, Netherlands, 833–840.

Lane DJ (1991) 16S/23S rRNA sequencing. In *Nucleic Acid Techniques in Bacterial Systematics* (eds Stackebrandt E, Goodfellow M). John Wiley and Sons, New York, pp. 115–175.

Lehman RM, Roberto FF, Earley D, Bruhn DF, Brink SE, O'Connell SP, Delwiche ME, Colwell FS (2001) Attached and unattached bacterial communities in a 120-meter corehole in an acidic, crystalline rock aquifer. *Applied and Environmental Microbiology* **67**, 2095–2106.

Leu JY, McGovern TCP, Porter AJR, Harris WJ, Hamilton WA (1998) Identification and phylogenetic analysis of thermophilic sulfate-reducing bacteria in oil field samples by 16S rDNA gene cloning and sequencing. *Anaerobe* **4**, 165–174.

López-Archilla AI, Marin I, Amils R (2001) Microbial community composition and ecology of an acidic aquatic environment: the Tinto River, Spain. *Microbial Ecology* **41**, 20–35.

Madsen EL (1995) Impacts of agricultural practices on subsurface microbial ecology. *Advances in Agronomy* **54**, 1–67.

Murphy SF (1995) Weathering of biotite in a tropical forest soil, Luquillo Mountains, Puerto Rico. MSc thesis, the Pennsylvania State University, University Park, PA.

Murphy SF, Brantley SL, Blum AE, White AF, Dong H (1998) Chemical weathering in a tropical watershed, Luquillo Mountains, Puerto Rico; II. Rate and mechanism of biotite weathering. *Geochimica et Cosmochimica Acta* **62**, 227–243.

Neubauer SC, Emerson D, Megonigal JP (2002) Life at the energetic edge: kinetics of circumneutral iron oxidation by lithotrophic iron-oxidizing bacteria isolated from the wetland-plant rhizosphere. *Applied and Environmental Microbiology* **68**, 3988–3995.

Núñez-Regueira L, Núñez-Fernández O, Rodríguez Añón JA, Proupín Castiñeiras J (2002) The influence of some physicochemical parameters on the microbial growth in soils. *Thermochimica Acta* **394**, 123–131.

Pimenov NV, Ivanova AE (2005) Anaerobic methane oxidation and sulfate reduction in bacterial mats on coral-like carbonate structures in the Black Sea. *Microbiology* **74**, 362–370.

Poszwa A, Dambrine E, Ferry B, Pollier B, Loubet M (2002) Do deep tree roots provide nutrients to the tropical rainforest? *Biogeochemistry* **60**, 97–118.

Reasoner DJ, Geldreich EE (1985) A new medium for the enumeration and subculture of bacteria from potable water. *Applied and Environmental Microbiology* **49**, 1–7.

von Blanckenburg F, Hewawasam T, Kubik PW (2004) Cosmogenic nuclide evidence for low weathering and denudation in the wet, tropical highlands of Sri Lanka. *Journal of Geophysical Research* **109**, F03008.

Richter DD, Markewitz D (1995) How deep is soil? *Bioscience* **45**, 600–609.

Richter DD, Oh NH (2002) Biological factors affecting saprolite formation. *Abstracts with programs – The Geological Society of America*, **34** Paper no. 48-4.

Riebe CS, Kirchner JW, Finkel RC (2003) Long-term rates of chemical weathering and physical erosion from cosmogenic nuclides and geochemical mass balance. *Geochimica et Cosmochimica Acta* **67**, 4411–4427.

Rohwerder T, Sand W, Lascu C (2003) Preliminary evidence for a sulphur cycle in Movile Cave, Romania. *Acta Biotechnologica* **23**, 101–107.

Schulz MS, White AF (1999) Chemical weathering in a tropical watershed, Luquillo Mountains, Puerto Rico; III. Quartz dissolution rates. *Geochimica et Cosmochimica Acta* **63**, 337–350.
Sheppard MI, Hawkins JL (1995) Iodine and microbial interactions in an organic soil. *Journal of Environmental Radioactivity* **29**, 91–109.
Sherr BF, Sherr EB, Fallon RD (1987) Use of monodispersed, fluorescently labeled bacteria to estimate in situ protozoan bactivory. *Applied and Environmental Microbiology* **53**, 958–965.
Sobolev D, Roden EE (2004) Characterization of a neutrophilic, chemolithoautotrophic Fe(II)-oxidizing β-proteobacterium from freshwater wetland sediments. *Geomicrobiology Journal* **21**, 1–10.
Stookey LL (1970) Ferrozine – A new spectrophotometric reagent for iron. *Analytical Chemistry* **42**, 779–781.
Sutherland RA (2002) Comparison between non-residual Al, Co, Cu, Fe, Mn, Ni, Pb and Zn released by a three-step sequential extraction procedure and a dilute hydrochloric acid leach for soil and road deposited sediment. *Applied Geochemistry* **17**, 353–365.
Taunton AE, Welch SA, Banfield JF (2000) Microbial controls on phosphate and lanthanide distributions during granite weathering and soil formation. *Chemical Geology* **169**, 371–382.
Turner BF, Stallard RF, Brantley SL (2003) Investigation of in situ weathering of quartz diorite bedrock in the Rio Icacos basin, Luquillo Experimental Forest, Puerto Rico. *Chemical Geology* **202**, 313–341.
USDA NCRS (2002) *Soil Survey of Caribbean National Forest and Luquillo Experimental Forest, Commonwealth of Puerto Rico*. pp. 181. USDA, Natural Resources Conservation Service. Washington, DC, USA.
White AF, Blum AE, Schulz MS, Vivit DV, Stonestrom DA, Larsen M, Murphy SF, Eberl D (1998) Chemical weathering in a tropical watershed, Luquillo Mountains, Puerto Rico: I. Long-term versus short-term weathering fluxes. *Geochimica et Cosmochimica Acta* **62**, 209–226.
Zelenev VV, van Bruggen AHC, Semenov AM (2005) Modeling wave-like dynamics of oligotrophic and copiotrophic bacteria along wheat roots in response to nutrient input from a growing root tip. *Ecological Modelling* **188**, 404–417.
Zhou J, Bruns MA, Tiedje JM (1996) DNA recovery from soils of diverse composition. *Applied and Environmental Microbiology* **62**, 316–322.
Zuberer DA (1994) Recovery and enumeration of viable bacteria. In *Methods of Soil Analysis, Part 2-Microbiological and Biochemical Properties* (ed. Weaver R). Soil Science Society of America, Madison, WI, pp. 119–144.